

X-ray time lags in the black hole candidates 1

2001

On the X-ray time lags in the black hole candidates

O. Kotov,^{2,1} E. Churazov,^{1,2} M. Gilfanov,^{1,2}

¹ *MPI für Astrophysik, Karl-Schwarzschild-Strasse 1, 85741 Garching, Germany*

² *Space Research Institute (IKI), Profsovnaya 84/32, Moscow 117810, Russia*

20 March 2001

ABSTRACT

It is shown that the energy dependence of the time lags in Cygnus X-1 excludes any significant contribution of the standard reflected component to the observed lags. The conclusion is valid in the 0.1–10 Hz frequency range where time lags have been detected with high enough significance. In fact the data hint that reflected component is working in opposite direction, reducing the lags at energies where contribution of the reflected component is significant.

We argue that the observed logarithmic dependence of time lags on energy can be understood as due to the small variations of the spectrum power law index in a very simple phenomenological model. We assume that an optically thin flow/corona, emitting a power law like spectrum, is present at a range of distances from the compact object. The slope of the locally emitted spectrum is a function of distance with the hardest spectrum emitted in the innermost region. If perturbations with different time scales are introduced to the accretion flow at different radii the observed X-ray lags naturally appear due to the inward propagation of perturbations on the diffusion time scales.

Key words: Accretion, accretion disks – Instabilities – Stars:binaries:general – Stars:classification X-rays: general – X-rays: stars

1 INTRODUCTION

Strong variability of the X-ray flux is a generic property of the black hole binaries in the so called hard state (see e.g. van der Klis 1994). While it is usually assumed that X-ray emission is produced via Comptonization of the low frequency photons by an optically thin cloud of hot electrons (e.g. Sunyaev and Truemper 1979) the nature of the strong variations is less well understood. One of the possible clues to the origin of the variability may be connected with the presence of the time lags between the light curves in different energy bands. The time lags were first found in the early observations of Cygnus X-1 (Priedhorsky et al. 1979, Nolan et al. 1981) and confirmed in the numerous subsequent observations of Cygnus X-1 and other black hole candidates. In the vast majority of cases hard photons lag with respect to the soft ones. From observations it was found that (i) the value of the time lag depends on frequency, (ii) time lag approximately logarithmically depends on the energy separation between two bands (e.g. Miyamoto & Kitamoto 1989), (iii) cross-correlation function between two bands peaks at zero lags within ~ 1 ms (Maccarone et al. 2000 and references therein). Comprehensive description of the observed Cygnus X-1 variability and time lags are given by Nowak et al., 1999a,b and Pottschmidt et al. 2000. A recent reviews of the observed lags and theoretical models are given by Poutanen 2001a,b.

We discuss below the time lags using RXTE data on Cygnus X-1 as the example. In Section 2 we show that observed energy dependence of the time lags excludes significant contribution of the standard reflected component to the time lags in Cygnus X-1. In Section 3 we introduce simple phenomenological model of the time lags, which naturally explains the logarithmic energy dependence of the time lags. In Section 4 we discuss the possibility of explaining the lags as due to diffusive propagation of the perturbations in the accretion flow. In Section 5 we discuss implications of the results. Section 6 summarizes our finding.

2 TIME LAGS DUE TO LIGHT CROSSING TIME OF THE REFLECTOR

For hard X-ray state of Cygnus X-1 one of the popular models assumes that an optically thick and geometrically thin disk is truncated at some radius from the compact object and most of the observed X-ray emission is coming from the more compact optically thin region located closer to the black hole (e.g. Esin, McClintock and Narayan 1997, Zdziarski et al. 1999). A fraction of the hard X-ray photons emitted by the central region can be intercepted by the optically thick disk and reemitted again. This re-emitted/reprocessed component, also called “reflected” component, has a very distinct spectral shape (e.g. Basko, Sun-

yaev & Titarchuk 1974, George & Fabian 1991). If matter in the optically thick disk is neutral or weakly ionized than the spectrum of the reflected component is harder (in the standard X-ray band) than the illuminating spectrum and it also contains prominent iron fluorescent K_α line. Because of the delay of photons which traveled from the emission region to the reflector and then to the observer hard lags may naturally appear (e.g. Poutanen 2001b).

In the presence of the direct and reflected components the observed spectrum $S(E, t)$ at time t can be written as:

$$S(E, t) = D(E, t) + R(E, t) \quad (1)$$

where $D(E, t)$ and $R(E, t)$ are the time dependent spectra of the direct and reflected components respectively. Assuming that the direct component vary in intensity only and not in shape:

$$D(E, t) = A(t)D(E) \quad (2)$$

and neglecting the dependence of the reflected component spectral shape on the incident and emission angles the reflected component can be written as:

$$R(E, t) = \frac{\Omega}{2\pi} R(E) \int T(\tau) A(t - \tau) d\tau \quad (3)$$

where $R(E)$ are the energy spectra of the reflected component calculated for the reflector subtending solid angle of 2π , $A(t)$ is the normalization of the direct component and $T(t)$ is the reflected component transfer function, which characterizes the time dependence of the intensity of the reflected component in response for a infinitely short flare of the direct component. In the above expression $T(t)$ is normalized such that $\int_0^\infty T(t) dt = 1$ and the contribution of the reflected component to the time averaged spectrum is expressed through the standard factor $\frac{\Omega}{2\pi}$, where Ω is the total solid angle subtended by the reflector. The expression (1) can be rewritten as:

$$S(E, t) = A(t)D(E) + \frac{\Omega}{2\pi} R(E) \int T(\tau) A(t - \tau) d\tau \quad (4)$$

Further assuming that contribution of the reflected component to the total spectrum is small one can write the expression for a frequency resolved spectrum, introduced in Revnivtsev et al. 1999:

$$\begin{aligned} S(E, f) &= |\hat{S}(E, f)| \approx \\ |\hat{A}(f)| D(E) &\times \sqrt{1 + 2 \frac{\Omega}{2\pi} \frac{R(E)}{D(E)} \text{Re}[\hat{T}(f)]} \approx \\ |\hat{A}(f)| &\times (D(E) + \frac{\Omega}{2\pi} R(E) \text{Re}[\hat{T}(f)]) \end{aligned} \quad (5)$$

The equivalent width of the iron line in the frequency resolved spectrum is then obviously:

$$EW(f) \approx EW_t \times \text{Re}[\hat{T}(f)], \quad (6)$$

where EW_t is the equivalent width in the total source spectrum. From the above expression it is clear that the equivalent width in the frequency resolved spectrum should decrease if the transfer function is smooth at a given frequency. E.g. when the light crossing time of the reflector is large the equivalent width should be low at the corresponding time scales. Using these arguments Revnivtsev et al. 1999, Gilfanov et al. 2000 set an upper limit on the effective size of

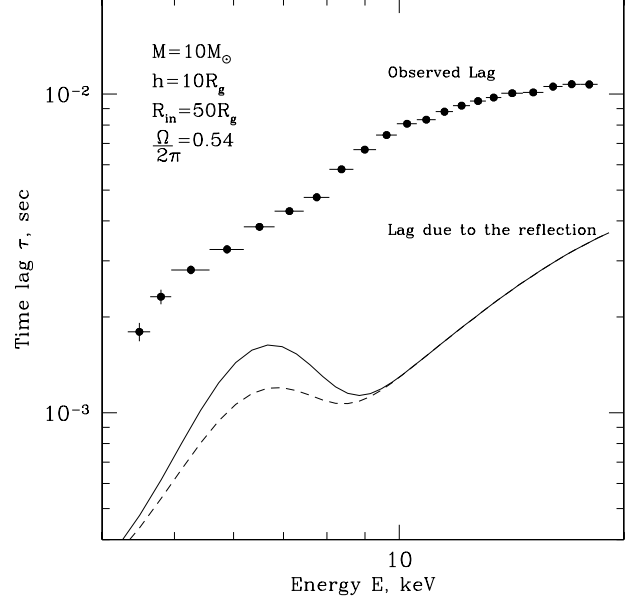


Figure 1. The energy dependence of the time lag in Cygnus X-1 in the hard state at the frequency of 2.5 Hz. For comparison the energy dependence of the time lags expected in the model with extended reflector is shown. For upper curve we used relative normalization of the Gaussian and reflected continuum obtained from the fit to the total Cygnus X-1 spectrum during observation 10238-01-08-00 (Gilfanov et al., 1999). For the lower curve the normalization of the Gaussian was chosen such that equivalent width of the line with respect to the reflected continuum is ~ 1 keV. The latter value is characteristic for an angle averaged reflection from a neutral matter with a normal abundance of heavy elements.

the reflector in Cygnus X-1 of $\sim 50 R_g$. We note here that the above expression assumes linear relation between variabilities in the reflected and direct components in the form of the convolution (3). If on the contrary the variability of the direct and reflected components are completely incoherent/unrelated then the contribution of the reflected component to the frequency resolved spectrum is proportional to square of the solid angle subtended by the reflector ($(\frac{\Omega}{2\pi})^2$).

One can further test the hypothesis of the large effective size of the reflector using the time lags. Assuming again that the light curve in any energy band can be expressed through (4) the expected phase lag $\phi(E, f)$ between given energy E and much lower energy (where contribution of the reflected component is negligible and the spectrum is solely due to direct component) can be written as:

$$\begin{aligned} tg(\phi(E, f)) &= \frac{\text{Im}[\hat{S}^*(E, f) \hat{D}(E, f)]}{\text{Re}[\hat{S}^*(E, f) \hat{D}(E, f)]} \approx \\ \frac{\frac{\Omega}{2\pi} R(E) \text{Im}[\hat{T}]}{D(E) + \frac{\Omega}{2\pi} R(E) \text{Re}[\hat{T}]} &\approx \frac{\Omega}{2\pi} \frac{R(E)}{D(E)} \text{Im}[\hat{T}(f)] \end{aligned} \quad (7)$$

Therefore in this approximation the frequency dependence of the phase/time lags is due to imaginary part of the Fourier transform of the transfer function. Energy de-

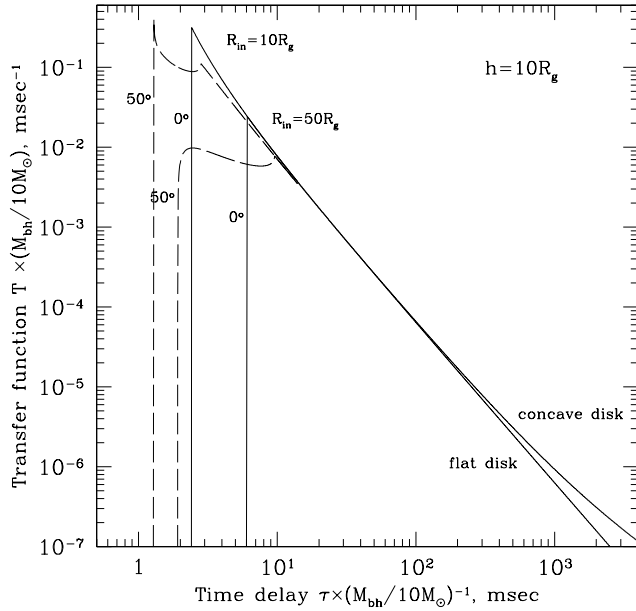


Figure 2. Transfer functions $\frac{\Omega}{2\pi}T(t)$ for an isotropic point source of primary radiation located at $h = 10R_g$ above a flat or concave disks with inner an radius of $R_{in} = 10$ and $50R_g$ and inclination of $0^\circ, 50^\circ$.

pendence of the lags is simply the ratio of the reflected and direct spectral components. Since $D(E)$ is assumed to be smooth function of energy the time/phase lag as the function of energy should contain prominent iron line with the equivalent width comparable with the equivalent width of the line in the reflected component, i.e. much larger equivalent width than in the total spectrum.

In order to assess possible contribution of the reflected component in the observed time lags in Cygnus X-1 we calculated lags in the narrow energy channels. For our analysis we use publicly available data of Rossi X-ray Timing Explorer observations P10238 performed between Mar. 26, 1996 and Mar. 31, 1996 with total exposure time ~ 70 ksec (we used only observations with all 5 PCU turned on). We used PCA data in the “Generic Binned” mode, having $\frac{1}{64}$ sec ~ 16 msec time resolution in 64 energy channels covering the whole PCA energy band (B_16ms_64M_0.249). The lags were calculated for every channel above 3.7 keV, with respect to the count rate in the 2.8-3.7 keV energy band. The resulting energy dependence of time lag at the frequencies of the order of 2.5 Hz is shown in Fig.1*. For comparison we plot in the same figure an expected energy dependence of the lags due to the reflected component, according to equation (7). Normalization of the expected curve is arbitrary. Here we used as $D(E)$ the averaged spectrum of the source during this observation. Reflected component $R(E)$ was calculated using XSPEC V11 (Arnaud 1996) model **pexrav** of Magdziarz & Zdziarski 1995 plus a Gaussian at the en-

ergy of 6.4 keV. The resulting spectrum has been convolved with the PCA energy response matrix. Note that expected lags were calculated using equation (7), i.e. with respect to the energy range where contribution of the reflected component was assumed to be zero. Therefore expected lags do not go to zero at the energy < 4 keV. Two curves shown in Fig.1 differ in the normalization of the Gaussian added to the reflected continuum. For upper curve we used relative normalization of the Gaussian and reflected continuum obtained from the fit to the total Cygnus X-1 spectrum during observation 10238-01-08-00 (Gilfanov et al., 1999). For the lower curve the normalization of the Gaussian was chosen such that the equivalent width of the line with respect to the reflected continuum is ~ 1 keV. The latter value is characteristic for an angle averaged reflection from a neutral matter with a normal abundance of heavy elements.

One can see from Fig.1 that the lags due to the reflected component should contain a prominent feature at the energy ~ 6.4 keV. We stress again that this feature should be much more prominent in the lags than in the averaged spectrum, where iron line provides at most 10% relative deviation of the observed spectrum from a power law fit. Clearly no such feature is present in the observed lags. We therefore conclude that the observed lags are predominantly not due to the reflected component.

One can use the same argument in order to constrain geometry of the reflecting region. Indeed lack of the iron line feature in the observed energy dependence of the time lags imply certain constraints on the combination of the reflected component strength and the duration of the time delay due to the finite size of the reflector. In the Fig.3 we show the observed energy dependence of the time lags at three representing frequencies: 0.6, 2.5 and 10 Hz. For comparison we show in the same plot expected time lags for different geometries of the reflector and different strength of the reflected component. Four basic models have been considered:

- **A:** A point isotropic source above the flat disk with the hole in the middle. The height h of the source above the disk plane is set to $10R_g$, the size of the hole R_{in} in the disk is set to $50R_g$. Here R_g is the gravitational radius for a $10M_\odot$ black hole. The factor $\Omega/2\pi$, calculated for this geometry, is $\simeq 0.2$.
- **B:** The same geometry as for **A**, but the strength of the reflected component was enhanced, so that effective parameter $\Omega/2\pi$ is 0.54. This is possible if e.g. the source of the primary emission is anisotropic and more emission is coming towards the disk than to the observer. Particular value of the normalization of the reflected component in this model was taken from the fit to the total Cygnus X-1 spectrum during observation 10238-01-08-00 (Gilfanov et al., 1999).
- **C:** The same geometry as for **A**, but for $R_{in} = 10R_g$. The factor $\Omega/2\pi$, calculated for this geometry, is $\simeq 0.7$.

The transfer functions in the form $\frac{\Omega}{2\pi}T(t)$ for models **A** and **C** are shown in Fig.2 for two values of the disk inclination θ (0° and 50°). Model **B** obviously has the same shape of the transfer function as model **A** and is different only in normalization. For comparison we also show the transfer function for a concave disk with the dependence of disk height over radius adopted from Shakura and Sunyaev (1973). For

* Time lags at other frequencies in the range from ~ 0.6 to ~ 10 Hz have approximately similar energy dependence (see Fig.3)

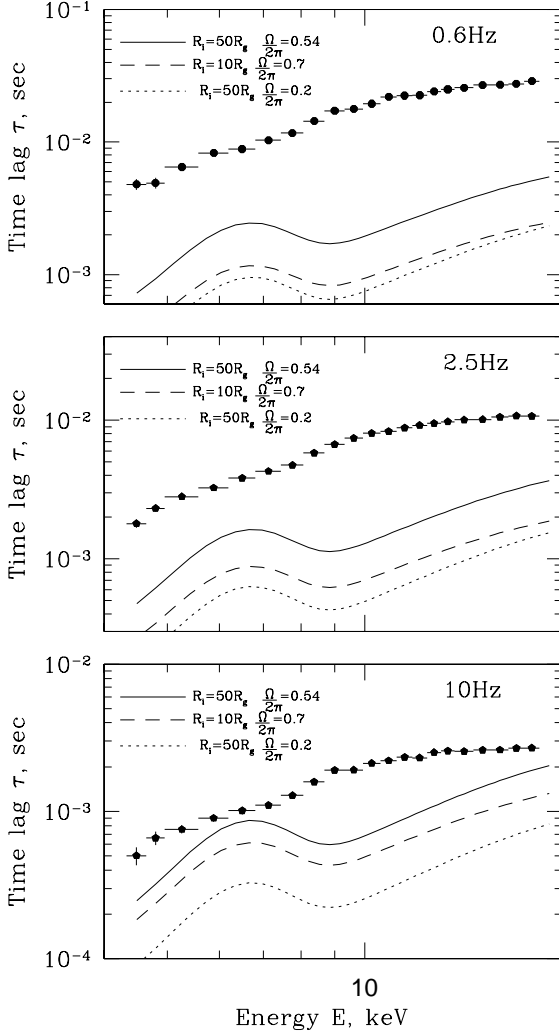


Figure 3. The energy dependence of the time lag in Cygnus X-1 in the hard state at different frequencies. For comparison we show the expected curves for the models where reflected component originates from a flat disk with a central hole illuminated by the compact source located at the height $h = 10R_g$ above the disk surface. The model curves were calculated for the equivalent width of the Fe K_α line obtained from the fit of the time averaged source spectrum.

the frequency range considered here such concave disks do not differ from the flat disks.

The lags expected in these models (for inclination $\theta = 50^\circ$) are shown in Fig.3. The model curves were calculated for the equivalent width of the Fe K_α line with respect to the reflected continuum obtained from the fit of the time averaged source spectrum. As was mentioned above lack of prominent iron feature in the energy dependence of the time lags suggests that lags are largely not due to the reflection. Moreover lags expected in models **B** and **C** at 10 Hz must produce clear feature at 6.4 keV in contradiction to the data. Even for model **A** expected lags can be only marginally “hidden” in the observed lags. There are however many uncertainties and simplifications in the models discussed above. In particular for simplicity we neglected the dependence of the reflected component spectrum on the incident angle. Also the surface of the reflector (upper few Thomson optical depths) may not be smooth and flat, but wrinkled. Furthermore ionization of the reflector surface will modify the spectrum of the reflected component. Finally all relativistic effects associated with reflection from the inner regions of the accretion disk (see e.g. Campana and Stella 1995) have been ignored. Account for all these effects may modify the normalization and shape of the energy dependence of the time lags by a factor of few.

Perhaps the most dubious assumption is the “linear” response of the reflected component to the variations of the illuminating flux. Recent analysis (e.g. Nayakshin and Kallman 2000) shows that shape of the reflected component can vary in a complicated fashion in response to increase of the primary flux. Therefore conservative conclusions of this section are that i) “linear” reflected component, containing prominent fluorescent line at 6.4 keV, is not responsible for the observed lags and ii) some of the source/reflector geometrical models can be definitely excluded.

3 TIME LAGS DUE TO VARIATIONS OF THE POWER LAW INDEX

The spectrum of Cygnus X-1 in the 2–20 keV energy band can be reasonably well approximated by a power law. Deviations, in particular due to the reflected component, are present, but their amplitude relative to the power law component is usually less than 10% in this energy range. We assume below that at any moment of time the spectrum can be represented as a power law:

$$S(E, t) = A(t)E^{-\alpha(t)} \quad (8)$$

where $A(t)$ is the normalization of the power law as a function of time and $\alpha(t)$ is the photon index, which is also a function time. For simplicity we set $\alpha(t) = \alpha_0 - \beta(t)$, where α_0 is a photon index of the time averaged spectrum and $\beta(t)$ is the time variable part of the photon index. Assuming that $\beta(t) \ll \alpha_0$ the spectrum of the source can be rewritten as:

$$S(E, t) = A(t)E^{-\alpha_0}(1 + \beta(t)\ln E) \quad (9)$$

The phase lag ϕ at a given frequency f can then be written through the Fourier transforms $\hat{S}^*(E, f)$ of the source

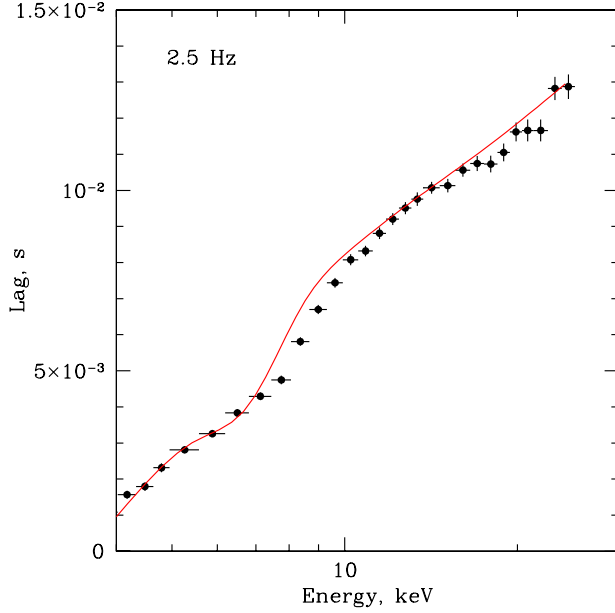


Figure 4. Time lag at the frequency of 2.5Hz as a function of $\text{Log}(E)$. See text for the description of the solid line.

light curves at two different energies E_1 and E_2 as:

$$\begin{aligned} \sin\phi &= \frac{\text{Im} [\hat{S}^*(E_1, f) \hat{S}(E_2, f)]}{|S(E_1, f)| |S(E_2, f)|} \approx \\ &= \frac{\text{Im} [(\hat{A}^* + (\hat{\beta}\hat{A})^* \ln E_1)(\hat{A} + (\hat{\beta}\hat{A}) \ln E_2)]}{\hat{A}^* \hat{A}} \approx \\ &= \frac{\text{Im} [\hat{A}^* (\hat{\beta}\hat{A})]}{\hat{A}^* \hat{A}} \times \ln \frac{E_2}{E_1} \end{aligned} \quad (10)$$

In the above expression we neglected terms of the order of $O(\beta^2)$. Thus the assumption that the spectrum has a power law shape at any moment of time and the variations of slope are small automatically implies that phase lags (and consequently time lags) scales as $\ln \frac{E_2}{E_1}$.

3.1 Universal slope flux correlation?

It is clear that if variations of slope $\beta(t)$ and normalization $A(t)$ are random and incoherent then the time lag is zero. If these two quantities are correlated then nonzero lag may appear. The simplest assumption would be a linear correlation between slope and normalization (i.e. between slope and flux):

$$\beta(t) = \gamma \times (A(t) - A_0) \quad (11)$$

where A_0 is the normalization of the time averaged spectrum and γ is the coefficient of linear proportionality between variations of normalization and slope.

The expression for phase lags is then further reduces to:

$$\sin\phi = \frac{\text{Im} [\hat{A}^* (\hat{A}^2)]}{\hat{A}^* \hat{A}} \times \gamma \ln \frac{E_2}{E_1} \quad (12)$$

In this approximation the sign and the amplitude of the lags would simply reflect properties of the flux variations on different time scales. Unfortunately the function (12), calculated for the observed light curves, changes the sign several times within the frequency range where hard lags are observed. This means that simple linear correlation between the flux and the slope of the spectrum can be excluded or that sign of the correlations between flux and slope also has to change sign in order to keep the sign of (12) the same at all frequencies. We note here that change of the slope/flux correlations sign at different time scales was indeed reported for Cygnus X-1 (Li, Feng & Chen 1999). Anyway it is clear that simple linear correlation between the slope and the flux fails to produce observed hard lags and more complicated models are to be invoked.

4 TIME LAGS DUE TO ACCRETION

In this section we construct simple model which attributes the lags to the propagation of perturbations in the accretion flow from the outer to inner region. As was discussed by Lyubarskii (1997) and Churazov, Gilfanov and Revnivtsev (2001) strong variability of the X-ray flux over very broad dynamic range of time scales suggests that different time scales are introduced to the accretion flow at different distances from the compact source. One might think e.g. in terms of the effect on the mass accretion rate of the magneto-hydrodynamic turbulence, which serves as a source of the viscosity in the accretion flow through the fluctuating magnetic stresses (e.g. Balbus and Hawley 1991, Hawley, Gammie and Balbus 1995, Brandenburg, Nordlund, Stein and Torkelsson 1995). The perturbations introduced at large distance from the compact object are then propagated down to the region of main energy release and cause observed variations of the X-ray flux. If the propagation of the perturbations in radial direction is due to viscous diffusion then the very fact that we observe strong variations of the X-ray flux means that propagation/diffusion time from a given radius r_0 is comparable to or shorter than the time scale of perturbations, introduced to the flow at this radius r_0 . Otherwise these perturbations would be completely washed out before reaching the innermost region. This in turn means that lags could naturally appear in such situation if locally emitted spectrum is a function of radius r . Of course energy budget of the accretion flow far from the innermost region is small, but the observed lags are also small, of the order of 0.1 radian. We then tested feasibility of this model using following assumptions:

- Statistically independent (incoherent) perturbations are introduced to the accretion flow at different distances from the compact source. The characteristic time scale of these perturbations is a function of radius.
- We further assume that the shape of the locally emitted spectra depends on radius and it is getting progressively softer with increase of the distance from the compact object.

The light curve at a given energy E is:

$$L(E, t) =$$

$$\int \int \int D(r_0, t_0) G(r, r_0, t - t_0) \epsilon(r) S(E, r) dr dr_0 dt_0 \quad (13)$$

where $D(r_0, t_0)$ is an initial perturbation introduced to the flow at radius r_0 and time t_0 , $G(r, r_0, t - t_0)$ is the Green function, which describes propagation of the perturbations from radius r_0 to r , $S(E, r)$ is the shape of the locally emitted spectrum at the radius r and $\epsilon(r)$ is the total luminosity of the accretion flow emitted at a given radius. Assumption of statistical independence of perturbations introduced at different radii implies that quantities like power density or cross spectra can be calculated independently for each initial radius and then averaged over range of initial radii. The Fourier transform $\hat{L}(E, f)$ of the X-ray light curve is then:

$$\hat{L}(E, f) = \int \hat{D}(r_0, f) \int \hat{G}(r, r_0, f) \epsilon(r) S(E, r) dr dr_0 \quad (14)$$

where $\hat{D}(r_0, f)$ is the Fourier transform of the perturbations introduced to the flow at the radius r_0 , $\hat{G}(r, r_0, f)$ is the Fourier transform of the Green function, f is the frequency. From the above equation it is clear that in this approximation time lags are solely due to the properties of the Green function and the dependence of the spectral shape on radius. For our toy model we choose the simplest possible version with $\epsilon(r) \propto 1/r^2$ per unit dr . In order to calculate phase and time lags we created two artificial light curves in the “soft” and “hard” bands assuming simple laws of emissivity in these bands:

$$S(r) = \epsilon(r) S(E_{soft}, r) = \frac{1}{r^2}$$

$$H(r) = \epsilon(r) S(E_{hard}, r) = \frac{1}{r^2} \times h(r) \quad (15)$$

where $h(r)$ is a decreasing function of the radius. For simplicity we assume that propagation of the perturbations can be characterized by the Green function of Lynden-Bell and Pringle (1974) describing diffusion in the geometrically thin disk approximation (see also Lyubarskii 1997). I.e.

$$G(r, r_0, t) \propto \frac{r^{-1/4}}{t} \exp \left[-\frac{r_0^{1/2l} + r^{1/2l}}{4t} \right] I_l \left[\frac{r^{1/4l} r_0^{1/4l}}{2t} \right] \quad (16)$$

where $I_\nu(x)$ is the Bessel function of imaginary argument. For the parameter l we use the value of $1/3$ appropriate for a standard α disk with constant ratio $\frac{H}{r}$, where H is a half thickness of the disk. In this equation and below we measure radius r in units of r_{min} , which is supposed to be the characteristic radius of the inner region of the accretion flow where most of the energy is released. Time is measured in units of the characteristic diffusion time $k^2 \times r_{min}^{1/2l}$, where k is the effective diffusion coefficient.

Two simple versions of the function $h(r)$ (hereafter “hardness” function) are shown in Fig.5. The dotted line shows the case when slope of the locally emitted spectrum is the same at all distances from the compact object, but it abruptly hardens within innermost region. The solid line shows the case when locally emitted spectrum gradually hardens as the distance from the compact object decreases. In Fig.5 light curves in the soft and hard energy bands are shown, assuming $h(r)$ function with the abrupt jump. Here initial radius r_0 was set to 30 and initial perturbation was assumed to be δ function in time and radius. Initially locally emitted spectrum is soft and it hardens when perturbation spreads all the way down to the minimal radius. After

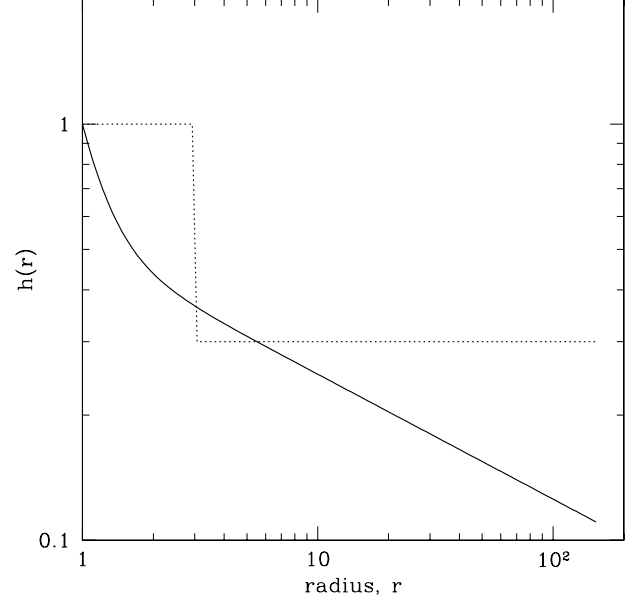


Figure 5. Two versions of $h(r)$ function, used in the simulations. Dotted line shows the $h(r)$ function when the locally emitted spectrum has the same slope at all distances from the compact object except for the innermost region, where the spectrum is harder. Solid line shows the case when spectrum gradually steepens with distance from the compact object. The amplitude of the $h(r)$ function change affects the absolute value of the time/phase lag.

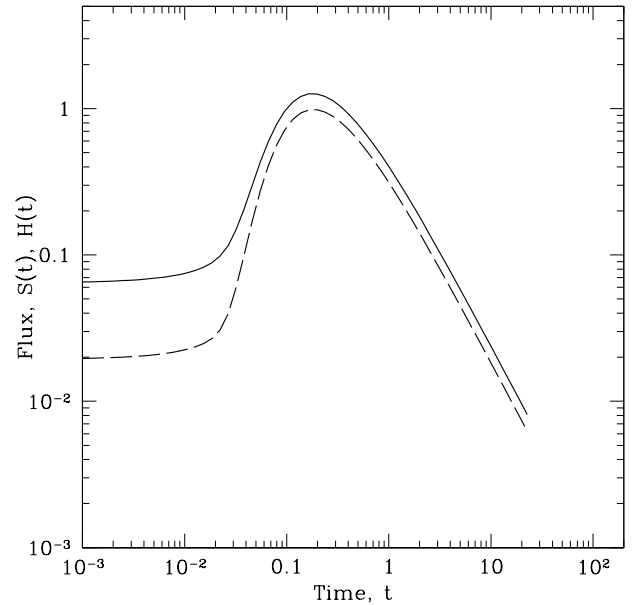


Figure 6. Light curves in two energy bands (soft – solid line, hard – dashed line) for the $\delta(t)$ perturbation at the initial radius $r_0 = 30$.

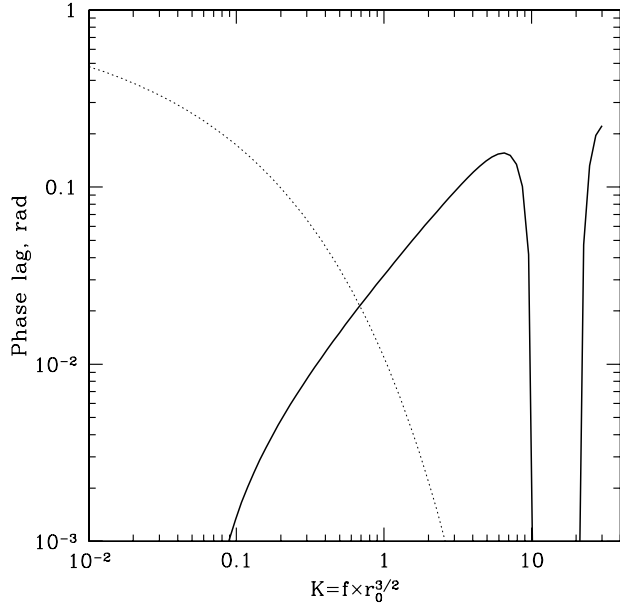


Figure 7. Phase lag (solid line) as a function frequency for the perturbations introduced at fixed initial radius $r_0 = 30$. Dotted line show the value of the transfer function power $|\int \hat{G}(r, r_0, f) \epsilon(r) dr|^2$, which characterizes the suppression of the power of the initial perturbation at a given frequency, due to diffusive spreading.

that moment hardness of spectrum remains practically unchanged.

We then calculated phase lags fixing the initial radius $r_0 = 30$ and varying the characteristic frequency of the initial perturbation. The dependence of the phase lag on frequency is shown in the Fig.7. Solid line in this figure shows the phase lag (in radians) as a function of frequency expressed in units of inverse characteristic diffusion time for a given initial radius $r_0^{3/2}$. These lags were calculated for $h(r)$ function with a jump (see Fig.5), but for the smoother $h(r)$ the resulting lags are practically the same. Dotted line in the same figure shows the value of the transfer function power $|\int \hat{G}(r, r_0, f) \epsilon(r) dr|^2$. It characterizes to what extent an amplitude of a perturbation at a given frequency f is suppressed in the observed light curve due to diffusive spreading. Values of the order of 10^{-2} imply that “local” perturbations at r_0 with an amplitude of the order of unity would result in $\sim 10\%$ variations in the innermost region where bulk of energy is released.

In order to calculate phase lags associated with the perturbations generated at different radii we made further simplifying assumption that at every initial radius r_0 instabilities generate single frequency which scales as a characteristic diffusion time at this radius[†]. I.e. $f(r_0) = K * r_0^{-3/2}$, where K is a parameter. From Fig.7 one would expect the lags

[†] Note that for the α disk with constant ratio of the disk height to the radius the characteristic diffusion time and Keplerian time scales similarly

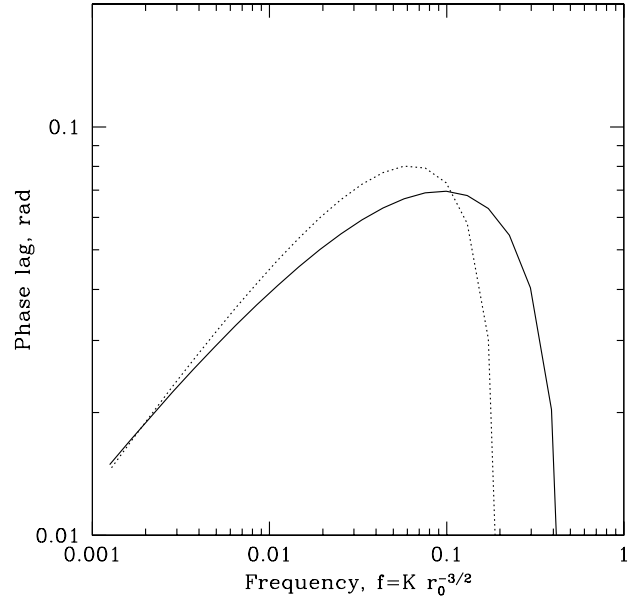


Figure 8. Phase lags for two versions of $h(r)$. Frequency, introduced at radius r_0 is assumed to scale as $K \times r_0^{-3/2}$ with $K = 1$.

to increase with the increase of K unless K is too large. The resulting phase lags for two versions of the “hardness” function are shown in the Fig.8. The resulting phase lags weakly grows with frequency and reach ~ 0.1 radian before falling sharply. The amplitude of the phase lags and the dependence of the lags on frequency are thus regulated by two major parameters: i) the strength of the spectral changes as a function of radius and ii) the relation between the time scale of perturbations, locally generated at radius r_0 , and diffusion time scales from r_0 down to much smaller radii. We stress that under assumption that at each radius r_0 perturbations with single characteristic frequency are generated the phase lags do not depend on the shape of the power density spectra and are solely determined by the Green function and the “hardness” function.

In the model, considered above, one would expect that power density spectra in different energy bands should have somewhat different shape due to the influence of the “hardness” function. In the Fig.9 we show the ratio of the power density spectra in the “hard” and “soft” bands as a function of frequency. This ratio is again independent on the shape of the power density spectrum and is governed by the the Green function and the “hardness” function. One can see that, as expected, the ratio of the power density spectra increases with frequency.

For completeness we also calculated time lags using the same choice of the “hardness” function, but instead of diffusion Green function we substitute Green function appropriate for a free fall from given radius r_0 . This is equivalent to the assumption that distinct blobs of emitting matter are falling towards the compact source with the velocity $v \propto r^{-1/2}$. The resulting lags are shown in Fig.10. Since in

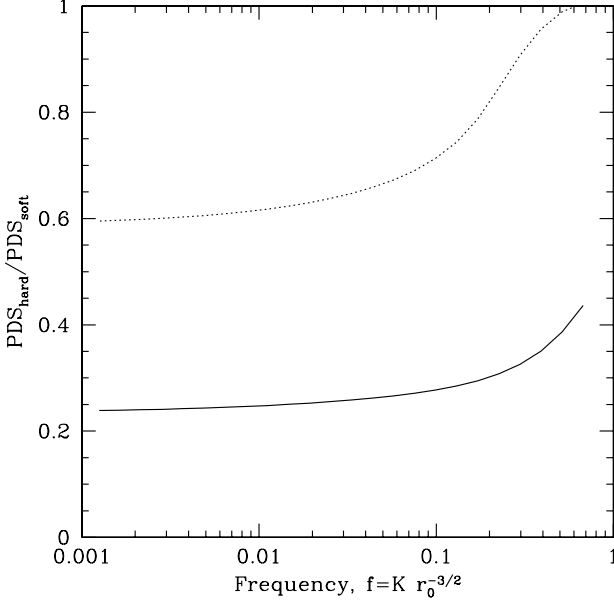


Figure 9. Ratio of the power density spectra of the hard and soft light curves (see eq.15) for two versions of $h(r)$.

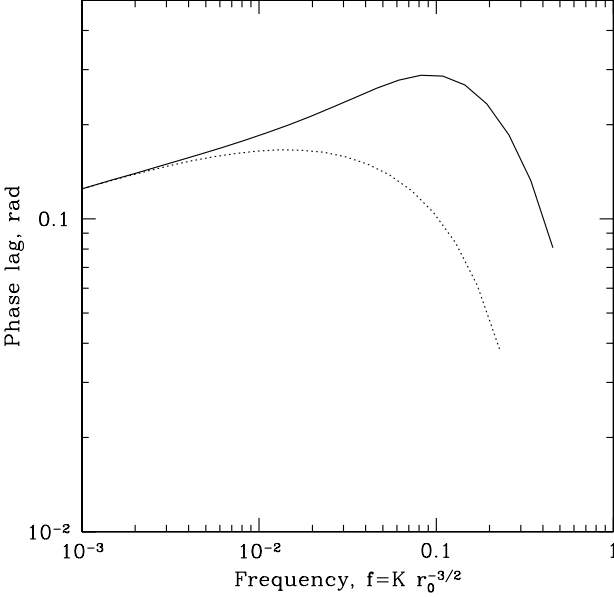


Figure 10. Lags for the free fall model for $K = 1$ and $K = 0.5$.

this case no viscous spreading is present, the absolute value of the lags is higher for the same choice of the “hardness” function and parameter K .

Finally we stress that if the locally emitted spectrum at any radii is a power law then observed lags will show logarithmic dependence on energy even if the total observed spectrum (integrated over all radii) is not well represented by a power law as assumed in the previous section. This follows from our assumption that perturbations generated at different radii are statistically independent.

4.1 “Antilags” due to reflected component

As we see in Section 2 observed energy dependence of the time lags contradicts the assumption that hard lags are predominantly produced by the time delay of the reflected component with respect to the primary continuum. In particular (see Fig.4) instead of a prominent hump at the energy of the iron fluorescent line the observed lags seem to be slightly suppressed here. This behavior might hint that reflected component somehow works in opposite direction and reduces the lags. We now discuss how such suppression could be introduced within the frame of the model considered above.

An assumption that locally emitted spectrum has a power law shape with an index slowly varying with the distance (so that hardest spectra are near the center) from the compact object will naturally lead to a hard lags with a logarithmic dependence of lags on energy. Let us now assume that locally emitted spectra also contain a reflected component. Assuming that overall geometry of the accretion flow resembles a truncated optically thick disk followed by an optically thin flow one would expect that the reflection fraction is higher for spectra emitted at larger distances from the compact object. I.e. softer spectra (emitted at larger distance from the compact object) have larger reflection fraction than harder spectra. In our model this means that reflected component is leading the harder spectrum. In this situation one would expect slight modification of the logarithmic dependence of lags on energy due to reflected component. The expected shape of the lags dependence on energy in this case is shown in Fig.4 with the solid line. For simplicity we assumed that lags are due to two power law spectra with the power law indices of 2.4 and 1.8 and the reflection fraction of ~ 1 and ~ 0.5 respectively. I.e. the light curve is:

$$L(E, t) = S_1(E) * \delta(t) + S_2(E) * \delta(t - \Delta t) \quad (17)$$

Reflected components in both spectra were smeared with a ~ 0.8 keV Gaussian. In the limit of small frequencies one can easily write an expression for the time lag as a function of energy for the light curve described by eq. (17). Detailed shape of the energy dependence is affected by strength of the reflection features in both spectra, amount of smearing applied, relative normalization of both spectra. One illustrative example, calculated for one particular choice of these parameters, is shown in Fig.4 with a solid curve. This curve is not supposed to closely reproduce the data, but just to demonstrate that the trend is in right direction.

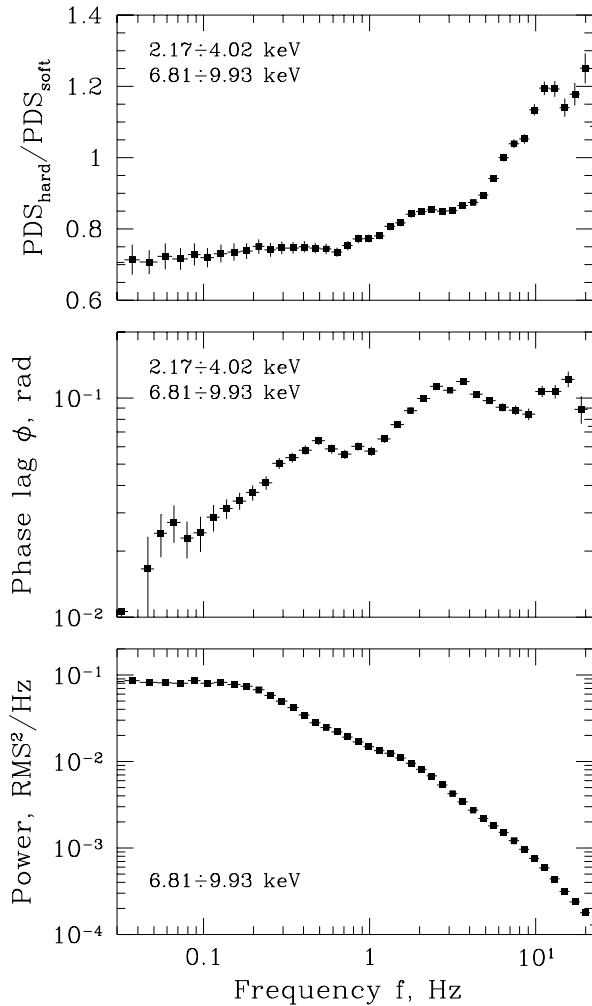


Figure 11. Cyg X-1: observed power density spectrum (lower panel), the phase lags (middle panel) and ratio of the power density spectra in the two energy bands (upper panel).

5 DISCUSSION

The properties of the hard lags, observed in Cyg X-1 can be summaries as following:

- In the hard state of Cygnus X-1 lags are observed very significantly in the frequency range of few 10^{-2} –few 10 Hz. Phase lag is a slightly growing function of frequency with a maximum phase lag of 0.1 rad between 3 and 10 keV (see recent data of Nowak et al. 1999a, Pottschmidt et al. 2000, also Fig.11).
- An energy dependence of the lags is approximately logarithmic (Miyamoto et al. 1988, Nowak et al. 1999a, see also Fig.4) with the slight, but statistically significant, deviations from this dependence.
- The cross correlation function peaks at zero lag (Maccarone et al. 2000).
- The coherence function is close to unity (Nowak et al. 1999a), at least in the middle of the frequency range, where lags are observed with high significance

Several different branches of models have been suggested as an explanation for the observed hard lags (see Poutanen 2001a,b for recent reviews). Our model belongs to the class of “propagation” models as defined by Nowak et al. 1999b. Other models involving “propagation” are those of Kato 1989, Nowak et al. 1999b, Böttcher and Liang 1999, Misra 2000, (see also Manmoto et al., 1996). In fact our version of the model is close to the original suggestion of Miyamoto et al. 1988, Miyamoto and Kitamoto 1989 that *a clump of matter ... drifts from the outer (soft-X-ray-emitting) region to the inner (hard-X-ray emitting) region.*

The model is based on two major assumptions: **a)** different time scales are introduced to the accretion flow at different distances from the compact object and propagation time scales are comparable to the time scales of perturbations and **b)** locally emitted spectra are power laws with the photon indices smaller in the innermost region.

The logarithmic energy dependence of the lags follows directly from the assumption **(b)**. Zero shift of the cross correlation function and coherence function close to unity naturally appear because most of the emission is coming from the innermost region and therefore most of the flux at all energies is released at the same time (see Fig.6). The dependence of the lags on frequency and maximal values of the lags are tunable parameters of the model (through the dependence of the photon index on the radius – the “hardness” function $h(r)$ and through the relation of the perturbation and propagation time scales). Examples shown above (see e.g. Fig.8) show that with reasonable assumptions one can approximately reproduce both the dependence of lags on frequency and the maximal value of the phase lag.

In addition this model provides natural explanation of the ratio of the power density spectra in different energy bands as a function of frequency (see Fig.9 and 11, upper panel) and offers a qualitative explanation for the deviations of the energy dependence of the lags from a simple logarithmic law (Fig.4). Broadly the model is consistent with the geometrical model in which the inside truncated optically thick disk is followed by the optically thin flow. At the distances larger than the disk truncation radius an optically thin flow seems to be also present and perhaps has a form of a corona sandwiching the disk (see arguments in Churazov et al. 2001). The latter assumption allows one to extend this model to the soft state of Cyg X-1 without any modifications.

Our assumption that each frequency in the observed flux variability is associated with some particular radius is of course a gross oversimplification. However due to suppression of the high frequency variations in the course of diffusion such situation may in practice materialize in the accretion flow if the times scales of locally induced perturbations at given radius are high, e.g. higher than the diffusion frequency (Churazov et al. 2001). From Fig.11 it is clear that there are several “humps” in the power density spectrum of Cyg X-1. Assuming that this is an indication that perturbations arising at some particular radius of the accretion flow are dominating at a range of frequencies one would then expect the phase lags to rise faster with frequency (compare Fig.8 and 7). It seems that such behavior is indeed observed as a distinct regions of fast phase lag rise (or time lag shoulders – see Nowak et al. 1999a,b) in the Cyg X-1 data (Fig.11).

Particular emission mechanism is not very important as long as only the origin of lags is considered. E.g. emission could be due to magnetic flares as in the picture of Galeev, Rosner, Viana 1979 or Poutanen and Fabian 1999. In our model flares spectra need not to evolve (from soft to hard) themselves. They could be short and could occur at different distances from the compact object. The observed variability could then be not due to individual flares but rather due to change of the number of active flares at a given moment of time. The model requires however that the spectra of a more distant flares to be softer than those of the flares in the innermost region of the accretion flow.

6 CONCLUSIONS

We show that some properties of the black hole candidates spectral variability in the X-ray band (in particular time lags) can be explained by a simple phenomenological model. This model assumes that **a)** different time scales are introduced to the accretion flow at different distances from the compact object and propagation time scales are comparable to the time scales of perturbations and **b)** locally emitted spectra are power laws with the photon indices smaller in the innermost region.

We also show that energy dependence of the time lags excludes the possibility that lags (in the 0.1 – 10 Hz range) are predominantly due to the delay of the reflected component with respect to the illuminating continuum. This conclusion is derived under assumption of a “standard” neutral reflected component which linearly responds to the variations of the illuminating flux.

7 ACKNOWLEDGEMENTS

This research has made use of data obtained through the High Energy Astrophysics Science Archive Research Center Online Service, provided by the NASA/Goddard Space Flight Center. O.Kotov acknowledges partial support by RFBR grant 00-15-96649.

REFERENCES

Arnaud K.A. 1996, *Astronomical Data Analysis Software and Systems V*, eds. Jacoby G. and Barnes J., p17, ASP Conf. Series volume 101.

Balbus, S. A. & Hawley, J. F. 1991, *ApJ*, 376, 214

Basko, M. M., Sunyaev, R. A., & Titarchuk, L. G. 1974, *A&A*, 31, 249

Böttcher, M. & Liang, E. P. 1999, *ApJ*, 511, L37

Brandenburg, A., Nordlund, A., Stein, R. F. and Torkelsson, U. 1995, *ApJ*, 446, 741

Campana, S. & Stella, L. 1995, *MNRAS*, 272, 585

Churazov, E., Gilfanov, M., & Revnivtsev, M. 2001, *MNRAS*, 321, 759

Esin, A. A., McClintock, J. E., & Narayan, R. 1997, *ApJ*, 489, 865

Galeev, A. A., Rosner, R. and Vaiana, G. S. 1979, *ApJ*, 229, 318

George, I. M. & Fabian, A. C. 1991, *MNRAS*, 249, 352

Gilfanov, M., Churazov, E., & Revnivtsev, M. 2000, *MNRAS*, 316, 923

Gilfanov, M., Churazov, E., & Revnivtsev, M. 1999, *A&A*, 352, 182

Hawley, J. F., Gammie, C. F. and Balbus, S. A. 1995, *ApJ*, 440, 742

Kato, S. 1989, *PASJ*, 41, 745

Li, T. P., Feng, Y. X., & Chen, L. 1999, *ApJ*, 521, 789

Lynden-Bell D. and Pringle J. E., 1974, *MNRAS*, 168, 603

Lyubarskii, Y. E., 1997, *MNRAS*, 292, 679

Maccarone, T. J., Coppi, P. S., & Poutanen, J. 2000, *ApJ*, 537, L107

Magdziarz, P. & Zdziarski, A. A. 1995, *MNRAS*, 273, 837

Manmoto, T., Takeuchi, M., Mineshige, S., Matsumoto, R., & Negoro, H. 1996, *ApJ*, 464, L135

Misra, R. 2000, *ApJ*, 529, L95

Miyamoto, S., Kitamoto, S., Mitsuda, K., & Dotani, T. 1988, *Nature*, 336, 450

Miyamoto, S. & Kitamoto, S. 1989, *Nature*, 342, 773

Nayakshin, S. & Kallman, T. R. 2001, *ApJ*, 546, 406

Nolan, P. L. et al. 1981, *ApJ*, 246, 494

Nowak, M. A., Wilms, J. J., Vaughan, B. A., Dove, J. B., & Begelman, M. C. 1999b, *ApJ*, 515, 726

Nowak, M. A., Vaughan, B. A., Wilms, J. J., Dove, J. B., & Begelman, M. C. 1999a, *ApJ*, 510, 874

Pottschmidt, K., Wilms, J., Nowak, M. A., Heindl, W. A., Smith, D. M., & Staubert, R. 2000, *A&A*, 357, L17

Poutanen, J. & Fabian, A. C. 1999, *MNRAS*, 306, L31

Poutanen, J. 2001, *X-ray Astronomy 1999, Stellar Endpoints, AGN and the Diffuse Background*, eds. G. Malaguti, G. Palumbo, and N. White, Gordon & Breach, Singapore, in press

Poutanen, J. 2001, *Advances in Space Research*, accepted

Priedhorsky, W., Garmire, G. P., Rothschild, R., Boldt, E., Serlemitsos, P., & Holt, S. 1979, *ApJ*, 233, 350

Revnivtsev, M., Gilfanov, M., & Churazov, E. 1999, *A&A*, 347, L23

Shakura N., Sunyaev R., 1973, *A&A*, 24, 337

Sunyaev R., Truemper J., 1979, *Nature*, 279, 506

van der Klis M., 1994, *ApJS*, 92, 511

Zdziarski, A. A., Lubinski, P., & Smith, D. A. 1999, *MNRAS*, 303, L11